Journal of Sound and Vibration (1985) **101**(2), 219-235

THE LOW FREQUENCY VIBRATION OF A RIBBED CYLINDER, PART 1: THEORY

C. H. HODGES, J. POWER AND J. WOODHOUSE

Topexpress Limited, 13/14 Round Church Street, Cambridge CB5 8AD, England

(*Received 24 May 1984, and in revised form 10 September 1984*)

The theory of vibrations of a cylinder braced by circular T-section ribs spaced regularly along its length is presented. Transmission experiments to validate the theory have been carried out on a ribbed cylinder model and these are described in an accompanying paper. Sufficiently detailed theoretical modelling of the ribs has enabled very good agreement between theory and experiment to be obtained.

1. INTRODUCTION

The modes of vibration of thin cylindrical shells have been studied by many authors. A number have also attempted to model such shells with supporting frames or ribs: see, for example, references [1-4] and other papers cited therein. In this paper a rather detailed theory is described, capable of treating the case of a cylindrical shell, of thickness h and radius a ($h \ll a$), which is braced by a large number of circular T-section ribs spaced regularly along its length with separation d. The treatment includes dynamical modelling of these ribs to allow for deformations of their cross-section during vibration. Figure 1 shows a sketch of the sort of geometry being studied, and defines notation for the various physical dimensions. Experiments have been carried out on a ribbed cylinder model of

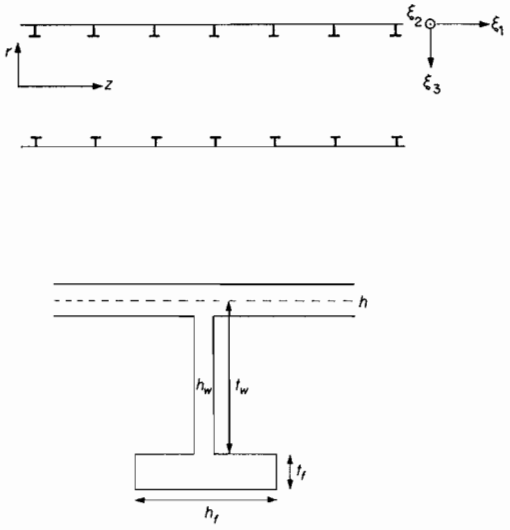

Figure 1. Sketch of the ribbed cylinder geometry, showing (above) an axial cross-section with axes and shell displacement components, and (below) an enlarged view of the rib cross-section defining the notation for the heights and widths of the web and flange.

0022-460X/85/140219+17 $03.00/0

this kind in order to validate the theoretical model described here. The results of those experiments and a comparison with the theory are described in the accompanying paper [5].

In this paper the freely propagating travelling waves on an infinite ribbed cylinder *in vacuo* are determined by using a method in which the effects of fluid loading can easily be incorporated in future work. Of course cylindrical structures of practical interest are of finite length, but they are often long enough that the infinite system gives a good idea of the transmission properties and general modal distribution on the finite structure. The precise determination of individual modal frequencies, which will not be attempted here, would necessitate the modelling of the ends of the cylinder. Approximate values for these frequencies can, however, be obtained by taking the travelling wave frequencies at discrete values of the wavenumber along the cylinder axis as described below.

In this introduction the general approach to the calculation is outlined. The treatment of periodicity is similar to that adopted by Mead and Pujara for periodically supported beams [6]. The treatment of cylindricality is based on work of Arnold and Warburton on thin cylindrical shells [7] to which extensive reference will be made throughout the present paper. It is convenient therefore to use the Arnold and Warburton notation and system of axes (see Figure 1) except that, instead of (u, v, w), (ξ_1, ξ_2, ξ_3) are used for the axial, tangential and radial (inward) displacements of a point on the middle surface of the shell, and the cylinder is taken to lie along the z- rather than the x-axis. Cylindrical polar co-ordinates (z, θ, r) are used.

The treatment of periodicity is greatly simplified by choosing to determine the travelling waves. For a cylinder of infinite length and rib spacing d, travelling wave solutions can be found which, so far as their z-dependence is concerned, have simple transformation properties of the form

$$\xi_i(z+md) = \mathrm{e}^{\pm \mathrm{i}qmd}\,\xi_i(z). \tag{1}$$

To use this result one clearly has to consider complex values for the spatial variation of displacement. If one does this the cylindrical symmetry also enables one to choose displacements whose angular dependence is of the form $\exp(\mathrm{i}n_c\theta)$ where n_c is an integer. Such displacements are of course combinations of solutions having the usual $\cos n_c\theta$, $\sin n_c\theta$ angular variation. Similarly, on a finite cylinder with simple boundary conditions the z-variation of modal displacement is a combination of the forward and backward travelling wave solutions above. The transformation property of travelling waves in a periodic system, equation (1), is a result known as Bloch's or Floquet's theorem [8]. It means for example that the axial variation of the shell displacement $\xi(z)$ can be factorized into $\exp(\pm \mathrm{i}qz)f(z)$ where $f(z)$ is periodic. This in turn means that the z-dependence of each ξ_i can be expressed as a Fourier series containing axial wavenumbers $q+2\pi n/d$ with integer values of n [6]. The Bloch wavenumber q is defined to be the wavenumber in this set which lies between π/d and $-\pi/d$, and it is denoted here by a different symbol from that of the conventional wavenumber k. Each of these Fourier components represents a diffracted wave produced by the "grating" of ribs. In the present problem Bloch's theorem can be viewed as a consequence of diffraction by the ribs, though in fact it is a rather more general result, valid also for systems of coupled pendula for example.

To calculate the travelling waves the Rayleigh-Ritz variational principle can be used with the Fourier coefficients of the shell displacements as variational parameters. In the absence of internal degrees of freedom for rib motion these coefficients determine not only the shell, but also the rib configuration and energy. In that case they provide a complete description of the problem provided enough Fourier components are included to model the wave shapes accurately. In the calculations presented here usually five terms

have been included in the expansion of each component of the shell displacement. Tests in which a larger number of terms were included showed no appreciable change in the results for mode frequencies in the range studied. Bending stiffness of the shell ensures that its displacement varies smoothly in space and the Fourier expansion must be rapidly convergent as was found by Mead and Pujara [6] for periodically supported bending beams.

The space harmonic representation of the shell displacement used here has two important advantages. First, one can write down the potential and kinetic energies of the cylindrical shell in terms of the Fourier coefficients by referring to the work of Arnold and Warburton [7] without needing to do any further calculation. In this approach the treatment of a ribbed cylinder is not very much more difficult than a ribbed flat plate, especially if the ribs are asymmetrically placed about the plate, when in-plane motions are coupled to normal motions for the plate as well as the cylinder. Second, the effect of fluid loading, to be included in future work, is easiest to take account of in the space harmonic representation, as has been pointed out recently by Mace in connection with studies of periodically stiffened, fluid-loaded flat plates [9, 10].

It is perhaps surprising that most of the difficulties in implementing this approach arose in connection with modelling the motion of individual ribs, in comparison to which periodicity and cylindricality were easily taken into account. As the calculations progressed the necessity of describing internal degrees of freedom of the ribs became evident. By an internal degree of freedom is meant a motion of the rib which can occur even if the cylindrical shell is held fixed. In the present case the most important one is a cantilever-like resonance of the flange and web sketched in Figure 2. The frequency of this resonance

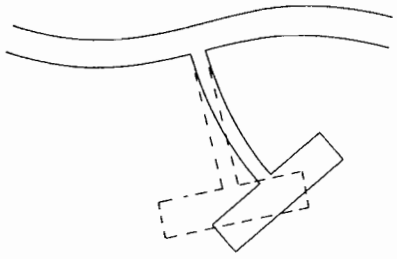

Figure 2. Sketch of a portion of the cylinder shell and rib cross-section for a (greatly exaggerated) typical motion. The dashed lines indicate the rib configuration in the absence of the cantilever internal degree of freedom.

increases with n_c but for our particular geometry it lies within the range of frequencies and n_c values studied. To incorporate this degree of freedom, the shape of the web during vibration is described by a cubic expression. The result is to introduce two more variational parameters, since the second and third radial derivatives of the web displacement are not directly related to the shell displacement. Together with the 15 generalized co-ordinates describing the shell (five Fourier coefficients in each of three Cartesian components of the shell displacement) this gives a total of 17 generalized co-ordinates to be varied. Applying the variational principle then leads to a 17×17 matrix eigenvalue problem for the travelling wave.

2. GENERAL APPROACH

The calculation in detail of the freely propagating waves on an infinite ribbed cylinder can now be started. In this section a suitable set of generalized co-ordinates is chosen.

This is followed by a discussion in general terms of how the potential and kinetic energies of the various components of the ribbed cylinder can be expressed in terms of those generalized co-ordinates, and some notation is introduced. The detailed calculation of the various energy terms is carried out in section 3, and the synthesis of those into the final variational model for which a computer program has been written is discussed in section 4. Some results of that program are presented and discussed in section 5.

As outlined in the previous section, the components of the cylinder displacement are described by sinusoidal θ variation and a Fourier series in z. It is convenient to take explicit account of the fact that the radial displacement ξ_3 is always in quadrature with the other two components (cf. Arnold and Warburton [7], equation (6)), and also to choose signs to achieve compatibility with Arnold and Warburton. Thus define

$$\xi_1 = -\sum_Q c_{1,Q} \exp[\mathrm{i}(Qz + n_c\theta)], \qquad \xi_2 = \sum_Q c_{2,Q} \exp[\mathrm{i}(Qz + n_c\theta)],$$
$$\xi_3 = \mathrm{i}\sum_Q c_{3,Q} \exp[\mathrm{i}(Qz + n_c\theta)], \tag{2}$$

where all the sums are taken over values of Q given by

$$Q = q + 2\pi n/d, \qquad n = 0, \pm 1, \pm 2, \ldots, \pm N_Q. \tag{3}$$

The series is usually truncated at $N_Q = 2$.

The three components of displacement at the root of the mth rib are equal to $d_i \exp(\mathrm{i}n_c\theta)$ times the factors -1, $+1$, i appearing in equation (2), where

$$d_i = \exp(\mathrm{i}qmd) \sum_Q c_{i,Q}, \qquad i = 1, 2, 3. \tag{4}$$

As mentioned in the previous section, it was found necessary in the course of developing this theoretical model to allow for some internal degrees of freedom of the individual ribs. Within the frequency range of interest, all that was needed was to allow the rib webs to bend in a way adequately modelled by allowing d_1 to vary with distance from the rib root according to the expression

$$d_1(x) = \exp(\mathrm{i}qmd) \sum_{\alpha=1}^{4} b_\alpha x^{\alpha-1}, \tag{5}$$

where $x = a - r$. The cubic expression represents static bending of the web exactly, and is thus an adequate approximation until the mass of the web begins to play a significant role in the dynamics of the vibration. Obviously for a more complete treatment or for different geometry one might have to make d_2 and d_3 depend on the co-ordinates in some similar way, but it will turn out that for the present problem the potential and kinetic energies associated with those components of motion can be calculated sufficiently accurately in terms of displacements at the root.

It is convenient to introduce two further variables to describe the rotation and axial displacement of the flange round the circumference. One writes $\phi_f \exp(\mathrm{i}n_c\theta)$ for the rotation and $d_f \exp(\mathrm{i}n_c\theta)$ for the axial displacement of the flange centre, where

$$\phi_f = \exp(\mathrm{i}qmd) \sum_{\alpha=1}^{4} (\alpha - 1) b_\alpha t_w^{\alpha-2}, \qquad d_f = (\phi_f t_f/2) + \exp(\mathrm{i}qmd) \sum_{\alpha=1}^{4} b_\alpha t_w^{\alpha-1}. \tag{6, 7}$$

Not all of the c's and b's introduced above are independent. At the root of each rib, the position and angle of tilt are determined by the cylinder motion by continuity requirements. These conditions mean that

$$b_1 = \sum_Q c_{1,Q}, \qquad b_2 = -\sum_Q Q c_{3,Q}. \tag{8}$$

It is clear that the potential and kinetic energies of the shell and ribs can ultimately be reduced to a quadratic form in the generalized co-ordinates $c_{i,Q}$, b_3 and b_4. One may then apply Rayleigh's principle in the usual way to obtain the frequency and form of each of the allowed travelling waves with the given n_c and q.

Both potential and kinetic energy are decomposed into a number of components for ease of calculation. First, one separates the total potential energy S into

$$S = S^s + S^r, \tag{9}$$

representing the contribution from the shell and the ribs respectively. Next, one can note an important consequence of symmetry. The effect of cylindrical and periodic symmetry has already been discussed. An isolated rib also possesses a mirror symmetry about the plane, normal to the cylinder axis, in which the rib lies. Motions having different reflection symmetries in this plane cannot be coupled by the rib. Thus symmetric in-plane motions, i.e., ξ_2 and ξ_3, are decoupled from antisymmetric axial motions ξ_1. (This is an example of a distinction which has been drawn in more general terms by Mead [11], in his division into "type (i)" and "type (ii)" coupling co-ordinates.) The modelling problem thus breaks down into two parts which may be treated separately, and one decomposes the rib potential energy into antisymmetric and symmetric contributions relative to the symmetry plane:

$$S^r = S^{ra} + S^{rs}. \tag{10}$$

The final subdivision one needs to make is that for the antisymmetric motions the contributions from the web and the flange are to be calculated separately. Thus one writes

$$S^{ra} = S^{wa} + S^{fa}. \tag{11}$$

The combined effect of these subdivisions is thus

$$S = S^s + S^{rs} + S^{wa} + S^{fa}, \tag{12}$$

and one similarly decomposes the kinetic energy:

$$T = T^s + T^{rs} + T^{wa} + T^{fa}. \tag{13}$$

In the next section the evaluation of these various terms is presented. It will turn out that S^s is naturally calculated as a quadratic form in the $c_{i,Q}$, while S^{rs} is initially calculated as a quadratic form in d_2 and d_3, and S^{wa} and S^{fa} are initially calculated as quadratic forms in the four b_α. Kinetic energy terms are of course similarly calculated. In section 4, one substitutes for the d's, b_1 and b_2 in terms of the set of generalized co-ordinates and gathers up terms to give the required overall quadratic forms for S and T.

3. EVALUATION OF POTENTIAL AND KINETIC ENERGY TERMS

3.1. MOTION OF THE SHELL

Since one wishes to apply the variational principle to the travelling waves satisfying equation (1), one is forced to consider complex displacements. Expressions for potential and kinetic energies must therefore be generalized to take account of this. For the potential energy of the cylindrical shell, equation (3) of Arnold and Warburton is generalized to

$$S^s = \frac{Ea}{2(1-\sigma^2)} \int\int\int \left[e_z^* e_z + e_y^* e_y + \sigma(e_z^* e_y + e_y^* e_z) + \left(\frac{1-\sigma}{2}\right) e_{zy}^* e_{zy} \right] \mathrm{d}\theta \, \mathrm{d}z \, \mathrm{d}r \tag{14}$$

where in the present notation the strain components are given by Arnold and Warburton as

$$e_z = \varepsilon_1 - x\kappa_1, \qquad e_y = \varepsilon_2 - x\kappa_2, \qquad e_{zy} = \gamma - 2x\tau \tag{15}$$

$$\varepsilon_1 = \partial\xi_1/\partial z, \qquad \varepsilon_2 = (1/a)(\partial\xi_2/\partial\theta - \xi_3), \qquad \gamma = \partial\xi_2/\partial z + (1/a)\partial\xi_1/\partial\theta,$$

$$\kappa_1 = \partial^2\xi_3/\partial z^2, \qquad \kappa_2 = (1/a^2)(\partial^2\xi_3/\partial\theta^2 + \partial\xi_2/\partial\theta), \qquad \tau = (1/a)(\partial^2\xi_3/\partial z\partial\theta + \partial\xi_2/\partial z). \quad (16)$$

Here x denotes radial distance (positive inwards) from the middle surface of the shell as before, E is Young's modulus, and σ is Poisson's ratio. The kinetic energy of the shell is similarly generalized.

In terms of the generalized co-ordinates $c_{i,Q}$ the potential energy of the shell is thus

$$S^s = \sum_Q \sum_{i,j} c^*_{i,Q} S^s_{ij}(Q) c_{j,Q} \quad (17)$$

per bay of the structure, where the matrix S^s_{ij} is given by

$$S^s_{11} = C^s[\lambda^2 + (1-\sigma)n_c^2/2], \qquad S^s_{12} = S^s_{21} = -C^s(1+\sigma)\lambda n_c/2,$$

$$S^s_{13} = S^s_{31} = C^s\sigma\lambda, \qquad S^s_{22} = C^s[(1-\sigma)(1+4\beta)\lambda^2/2 + (1+\beta)n_c^2],$$

$$S^s_{23} = S^s_{32} = -C^s n_c\{1+\beta[n_c^2 + (2-\sigma)\lambda^2]\}, \qquad S^s_{33} = C^s[1+\beta(\lambda^2+n_c^2)^2], \quad (18)$$

$$C^s = \pi Ehd/a(1-\sigma^2), \qquad \lambda = Qa, \qquad \beta = h^2/12a^2. \quad (19)$$

The matrix elements S^s_{ij} are real, and lead to equations of motion for the shell identical in form to those in the Appendix of Arnold and Warburton.

Similarly, the kinetic energy per bay is

$$T^s = \omega^2 \pi\rho ahd \sum_Q \sum_i c^*_{i,Q} c_{i,Q}, \quad (20)$$

where ρ is the volume density of the shell.

3.2. SYMMETRIC IN-PLANE MOTION OF THE RIBS

For in-plane motion of the ribs, the appropriate expression for potential energy in terms of strain components is that for beam theory, suitably generalized to allow for complex displacements:

$$S^{rs} = \tfrac{1}{2}Ea \int \mathrm{d}\theta \int \mathrm{d}x\, l(x)\left[e^*_y e_y + \frac{1}{2(1+\sigma)} e^*_{xy} e_{xy}\right]. \quad (21)$$

Here $l(x)$ represents the rib profile: i.e., its width in the axial direction as a function of distance measured inwards from the middle surface of the shell. It will turn out to be important that this profile is asymmetric with respect to the middle surface of the shell—this will be discussed in section 5 when some results from the complete theoretical model are examined.

The first term in equation (21) corresponds to the normal theory for the bending and extension of thin beams. The second term represents shearing motion. It was found necessary to retain this term and use a treatment analogous to Timoshenko beam theory (see e.g., reference [12], p. 109 ff.). The reason for this lies in the detailed geometry of the ribs. The thinness of the web means that the potential energy of stretching of the rib flange can be accommodated to a considerable extent by shear in the rib web. Thus the shear correction is significant at much lower frequencies than would be the case for rectangular section ribs but, on the other hand, the simple Timoshenko-like treatment is adequate over a larger frequency range than would normally be the case (see reference [12], *loc. cit.*).

The potential energy of the rib for in-plane motion can now be discussed, with the shear contribution neglected, as was done in the initial calculations. The effect of shear is discussed in the Appendix. For the moment then, the second term in equation (21) is

neglected and the first term evaluated by using equations (15) and (16) for e_y, ε_2, κ_2 which give the compressional strain variation through a thin beam in which there is no shear. Thus S^{rs} becomes

$$S^{rs} = \tfrac{1}{2}Ea \int \mathrm{d}\theta [I_1(\varepsilon_2^* \varepsilon_2) - I_x(\varepsilon_2^* \kappa_2 + \varepsilon_2 \kappa_2^*) + I_{x^2}(\kappa_2^* \kappa_2)], \tag{22}$$

where I_1, I_x and I_{x^2} are the moments of the rib profile, defined by

$$I_1 = \int l(x)\,\mathrm{d}x, \qquad I_x = \int xl(x)\,\mathrm{d}x, \qquad I_{x^2} = \int x^2 l(x)\,\mathrm{d}x. \tag{23}$$

Now one substitutes equations (15) and (16) for ε_2 and κ_2 and notes that, at the rib, ξ_i is equal to $d_i \exp(\mathrm{i}n_c\theta)$ multiplied by the factor -1, $+1$, or i as in equation (2). One then obtains

$$S^{rs} = S^{rs}_{22}(d_2^* d_2) + S^{rs}_{23}(d_2^* d_3 + d_3^* d_2) + S^{rs}_{33}(d_3^* d_3), \tag{24}$$

$$S^{rs}_{22} = C^{rs} n_c^2 [I_1 - (2I_x/a) + (I_{x^2}/a^2)],$$

$$S^{rs}_{23} = -C^{rs} n_c [I_1 - (n_c^2 + 1)(I_x/a) + (n_c^2 I_{x^2}/a^2)],$$

$$S^{rs}_{33} = C^{rs}[I_1 - (2n_c^2 I_x/a) + (n_c^4 I_{x^2}/a^2)], \tag{25}$$

$$\text{where } C^{rs} = \pi E/a, \tag{26}$$

and d_2 and d_3 are the rib tangential and radial displacement co-ordinates. One can note in passing two features of this expression. The first is the absence of the factor $(1-\sigma^2)$, which occurs in plate theory but not in beam theory. This arises because the tendency of Poisson's ratio to produce "contrary curvatures" can operate freely in a beam but is constrained in a plate. The second is the existence of terms depending on the first moment of the rib cross-section I_x, which arise from the asymmetry of the rib with respect to the middle surface of the shell as mentioned above. The effect of shear is discussed in the Appendix. The main result derived there is that shear is included simply by replacing I_1, I_x, I_{x^2} in equation (25) by J_1, J_x, J_{x^2} defined by equation (A12).

The kinetic energy of in-plane rib motion can be approximated by

$$T^{rs} = \frac{\omega^2 a m^r}{2} \int \mathrm{d}\theta(\xi_2^* \xi_2 + \xi_3^* \xi_3) = \omega^2 \pi a m^r (d_2^* d_2 + d_3^* d_3), \tag{27}$$

where $m^r = \rho I_1$ is the mass per unit length of the rib. In this approximation the kinetic energy is treated as if all the mass of the rib were concentrated at the middle surface of the shell. Corrections to this result could be included quite easily, but as far as can be seen they are of rather minor importance.

3.3. ANTISYMMETRIC AXIAL MOTION OF THE RIBS

The detailed modelling of the rib is even more crucial as far as axial motion is concerned because of the existence of a cantilever resonance of the rib flange and web which lies in the frequency range of interest. This resonance does not just shift frequencies but introduces a new band into the dispersion curve as will be seen in section 5.

One can first treat the web. This forms a thin flat plate of annular form, so that its potential and kinetic energies may be expressed immediately in terms of its normal displacement (see, for example, the book by Rayleigh [13], § 214). One could thus evaluate both energy terms completely from the assumed form for the normal displacement from equation (5). However, since the web is narrow compared to its mean radius and thin

compared to the flange, it is sufficiently accurate to use the approximate expression

$$S^{wa} \simeq \frac{\pi E a h_w^3}{12(1-\sigma^2)} \int_0^{t_w} d_1''(x)^* d_1''(x)\, \mathrm{d}x. \tag{28}$$

The web kinetic energy is given by

$$T^{wa} \simeq \omega^2 \pi \rho a h_w \int_0^{t_w} d_1(x)^* d_1(x)\, \mathrm{d}x. \tag{29}$$

Substituting equation (5) into equation (28) gives for the potential energy

$$S^{wa} = \sum_{\alpha\beta} b_\alpha^* S_{\alpha\beta}^{wa} b_\beta, \qquad S_{\alpha\beta}^{wa} = \frac{\pi E a h_w^3 t_w^{\alpha+\beta-5}}{12(1-\sigma^2)} \frac{(\alpha-1)(\alpha-2)(\beta-1)(\beta-2)}{\alpha+\beta-5} \tag{30, 31}$$

(zero if either α or β is 1 or 2). Similarly, one can define a matrix

$$T_{\alpha\beta}^{wa} = \pi \rho a h_w t_w^{\alpha+\beta-1}/(\alpha+\beta-1) \tag{32}$$

for which the quadratic form corresponding to equation (30) gives the kinetic energy when multiplied by ω^2.

One can now treat the flange. For the sort of geometry illustrated in Figure 1, h_f is substantially larger than t_f and it is therefore appropriate to treat the flange as an element of a cylindrical shell (radius a_f). Apart from one minor modification to be discussed below, its potential energy can be deduced from equation (14) for thin shell theory. One starts by minimizing statically with respect to e_z to obtain

$$S^{fa} = \frac{E a_f}{2} \int\int\int \left[e_y^* e_y + \frac{1}{2(1+\sigma)} e_{zy}^* e_{zy} \right] \mathrm{d}\theta\, \mathrm{d}z\, \mathrm{d}r, \tag{33}$$

in the same way that one obtains equation (21) for the symmetric in-plane motion of the rib. Provided $h_f < a_f / n_c$ the bending associated with the axial motion of the flange obeys thin beam theory. There is therefore no shear in the middle surface: i.e., γ in equation (16) must vanish. This condition allows one to determine the remaining non-zero strain components in terms of d_f and ϕ_f, the flange displacement and rotation co-ordinates introduced in section 2. Since one is considering antisymmetric motion the axial, tangential and radial displacements are given by

$$\xi_1 = -d_f \exp(\mathrm{i} n_c \theta), \qquad \xi_2 = -(z/a_f)\partial\xi_1/\partial\theta, \qquad \xi_3 = z\phi_f \exp(\mathrm{i} n_c \theta), \tag{34}$$

where z is the axial displacement from the flange centre. On substituting into equations (16) and (17) and then into equation (33), integrating through the flange cross-section and round the circumference, one obtains

$$S^{fa} \simeq \frac{\pi E h_f t_f}{12 a_f} \left[h_f^2 \left(\phi_f + \frac{n_c^2}{a_f} d_f \right)^* \left(\phi_f + \frac{n_c^2}{a_f} d_f \right) + \Gamma t_f^2 n_c^2 \left(\phi + \frac{1}{a_f} d_f \right)^* \left(\phi_f + \frac{1}{a_f} d_f \right) \right], \tag{35}$$

$$a_f = a - h/2 - t_w - t_f/2, \qquad \Gamma = 2/(1+\sigma). \tag{36}$$

The term proportional to κ_2^2 is in comparison negligible provided $h_f < a_f / n_c$.

In this derivation the in-plane strain assumption common to thin shell theories has been made (i.e., terms involving shear components e_{xy} as in equation (21) are neglected). By analogy with the theory of the torsional rigidity of bars of rectangular cross-section [14], it is clear that this assumption must break down within a distance of the order of t_f from the side faces of the flange, the effect being to reduce the rigidity. For the present circular flange geometry Γ in equation (35) may be reduced in an *ad hoc*, if plausible,

fashion by using the factor appropriate to a straight bar (reference [12], p. 93). This correction has been found to make remarkably little difference to the results but it is included in the final calculations.

In terms of the variables ϕ_f, d_f, the kinetic energy of the rib flange is

$$T^{fa} = \omega^2 \pi \rho a_f h_f t_f (d_f^* d_f + R_f^2 \phi_f^* \phi_f), \tag{37}$$

where $R_f^2 = (h_f^2 + t_f^2)/12$ defines the radius of gyration of its cross-section.

One may define potential and kinetic energy matrices for the flange by substituting equations (6) and (7) in equations (35) and (37). The potential energy is then

$$S^{fa} = \sum_{\alpha\beta} b_\alpha^* S_{\alpha\beta}^{fa} b_\beta, \tag{38}$$

$$S_{\alpha\beta}^{fa} = (\alpha-1)(\beta-1) t_w^{\alpha+\beta-4} S'_{\phi\phi} + (\alpha+\beta-2) t_w^{\alpha+\beta-3} S'_{\phi d} + t_w^{\alpha+\beta-2} S_{dd},$$

$$S'_{\phi\phi} = S_{\phi\phi} + t_f S_{\phi d} + \tfrac{1}{4} t_f^2 S_{dd}, \qquad S'_{\phi d} = S_{\phi d} + \tfrac{1}{2} t_f S_{dd}, \tag{39}$$

with $S_{\phi\phi}$, etc., the coefficients in the expansion of equation (35), being given by

$$S_{\phi\phi} = (\pi E h_f t_f / 12 a_f)(h_f^2 + \Gamma t_f^2 n_c^2), \qquad S_{\phi d} = (\pi E h_f t_f / 12 a_f^2)(h_f^2 + \Gamma t_f^2) n_c^2,$$

$$S_{dd} = (\pi E h_f t_f / 12 a_f^3)(h_f^2 n_c^4 + \Gamma t_f^2 n_c^2). \tag{40}$$

In a similar fashion the flange kinetic energy defines a matrix $\omega^2 T_{\alpha\beta}^{fa}$ obtained by substituting the coefficients of the expansion of equation (37),

$$T_{\phi\phi} = \pi \rho a_f h_f t_f R_f^2, \qquad T_{\phi d} = 0, \qquad T_{dd} = \pi \rho a_f h_f t_f, \tag{41}$$

in the places of $S_{\phi\phi}$, $S_{\phi d}$, S_{dd}, in equation (39).

4. COMPUTATION OF THE COMPLETE MODEL

One can now reduce all potential and kinetic energies to quadratic forms in the basic generalized co-ordinate set as described at the end of section 2. One therefore substitutes equation (4) in equation (24), equation (8) in equations (30) and (38), etc., and collects up terms including equation (17) for the shell. Applying Rayleigh's variational principle gives a matrix eigenvalue equation for the travelling waves and their frequencies. This equation is presented here in the form in which it appears in the computer program developed to do the calculation. To do this one must number the generalized co-ordinates. One thus defines

$$n_i = n - N_Q + i(2N_Q + 1), \qquad n'_j = n' - N_Q + j(2N_Q + 1). \tag{42}$$

Here n and n' run between $\pm N_Q$ which defines the truncation of the Fourier series in equation (2). Now n_i and n'_j are the numbers assigned to the co-ordinates $c_{i,Q}$ and $c_{j,Q'}$ with $Q = q + 2\pi n/d$ and $Q' = q + 2\pi n'/d$. In addition

$$m_3 = 3(2N_Q + 1) + 1, \qquad m_4 = 3(2N_Q + 1) + 2 \tag{43}$$

are the numbers assigned to the co-ordinates b_3 and b_4.

The matrix eigenvalue equation has the form

$$\sum_{j=1}^{m_4} [S(q) - \omega(q)^2 T(q)]_{ij} c_j = 0, \tag{44}$$

where c is the eigenvector, $\omega(q)^2$ the eigenvalue and the matrices $S(q)$ and $T(q)$ have rank m_4 (usually 17). The matrix elements of $S(q)$ and $T(q)$ are related to the matrices

given in equations (18), (25), (31) and (39) and are defined as follows:

$$S(n_1, n_1') = S_{11}^{ra} + S_{11}^{s}\delta_{nn'}, \qquad S(n_1, n_2') = S_{12}^{s}\delta_{nn'}, \qquad S(n_1, n_3') = -(q+2\pi n'/d)S_{12}^{ra} + S_{13}^{s}\delta_{nn'},$$
$$S(n_2, n_2') = S_{22}^{rs} + S_{22}^{s}\delta_{nn'}, \qquad S(n_2, n_3') = S_{23}^{rs} + S_{23}^{s}\delta_{nn'},$$
$$S(n_3, n_3') = S_{33}^{rs} + (q+2\pi n/d)(q+2\pi n'/d)S_{22}^{ra} + S_{33}^{s}\delta_{nn'},$$
$$S(n_1, m_\beta) = S_{1\beta}^{ra}, \qquad S(n_2, m_\beta) = 0,$$
$$S(n_3, m_\beta) = -(q+2\pi n/d)S_{2\beta}^{ra}, \qquad S(m_\alpha, m_\beta) = S_{\alpha\beta}^{ra}, \tag{45}$$

where α and β now run from 3 to 4, and S_{ij}^{s} depends implicitly on $Q = q + 2\pi n/d$ via equations (18) and (19). $S(1, 1)$ is used to denote the matrix element S_{11} and so on, simply to avoid having subscripts of subscripts. These equations completely define the matrix S since it is symmetric. The kinetic energy matrix T is defined by substituting on the right-hand side of equation (45) matrices obtained from equations (20), (27), (32) and (37). These are given by

$$T_{ij}^{s} = \pi\rho ahd\delta_{ij}, \qquad i, j = 1, 2, 3, \qquad T_{ij}^{rs} = \pi a m^{r}\delta_{ij}, \qquad i, j = 2, 3 \tag{46, 47}$$

while $T_{\alpha\beta}^{ra}$ is the sum of equation (32) and the matrix obtained by substituting equation (41) in equation (39).

A computer program has been developed to calculate the matrices $S(q)$ and $T(q)$, and thus to determine the eigenvalues and eigenvectors corresponding to equation (44). In the next section some results of numerical calculations are presented and discussed, but the bulk of the results and discussion is saved for the companion paper [5], where comparisons are made with measurements. There is one small point about some of these results which should be noted here: sometimes not only the frequency $\omega(q)$ is required but also the group velocity $\mathrm{d}\omega(q)/\mathrm{d}q$. The latter could be obtained by numerically differencing the ω's for nearby q values, but more accurate values can be obtained as follows. For a small increment in wavenumber δq the change in eigenvalue $\delta\omega^2$ is determined by $\delta S(q)$ and $\delta T(q)$, the increments of the matrices in equation (44). From first order perturbation theory one therefore obtains

$$\frac{\mathrm{d}\omega}{\mathrm{d}q} = \frac{1}{2\omega}\sum_{i,j}\left(\frac{\mathrm{d}S}{\mathrm{d}q} - \omega^2\frac{\mathrm{d}T}{\mathrm{d}q}\right)_{ij} c_i c_j, \tag{48}$$

where the matrix in round brackets is obtained by differentiating equation (45) with account being taken of the implicit q dependence of S_{ij}^{s} ($\sum_{i,j} T_{ij}c_i c_j$ is normalized to unity).

5. RESULTS

The main problem with presenting the results of the numerical calculations is that there is a lot of information to convey, and this cannot all be shown on any one picture. Thus three different types of plot are used in an attempt to highlight important aspects of the behaviour. The first shows frequency against n_c for two values of axial Bloch wavenumber, $q = 0$ and $q = \pi/d$ (Nyquist), and the second shows frequency against axial wavenumber q for fixed n_c. Between them these two show the pattern of stop and pass bands arising from the periodic structure, in its dependence on the two components of wavenumber, axial and circumferential. The third type of plot shows inverse group velocity against frequency, and examples are shown in the accompanying paper, where they provide theoretical comparison with experimental sonograms [15]. The frequency axis of all these

plots is marked in units of the ring frequency

$$f_r = (1/2\pi a)[E/\rho(1-\sigma^2)]^{1/2}, \tag{49}$$

and they all cover a range from 0 to $3f_r$.

There is another aspect of the results which one would also like to see: namely the forms of the mode shapes corresponding to the different modal frequencies. It is very hard to show these in any complete way, but an attempt has been made to give some relevant information on the same pictures. As explained in the accompanying paper [5], in the measurements the cylinder was excited in three different positions in order to focus attention on different types of motion: radially on a rib, radially at mid-bay and axially on a rib flange. Therefore it is shown for each mode which of these three measurement positions should give the strongest response, by using three different plotting symbols: a square denotes that radial motion on the rib is strongest, a diamond, radial motion in mid-bay, and a circle, axial motion on the rib flange. Thus one has calculated d_3, ξ_3 at mid-bay, and d_f from equations (4), (2) and (7), determined which is largest in amplitude, and plotted accordingly. While this approach to showing mode shape information works fairly well, there are inevitably some undesirable side-effects. In particular, there are some modes for which the motion is primarily within the shell surface. In such cases, the motion

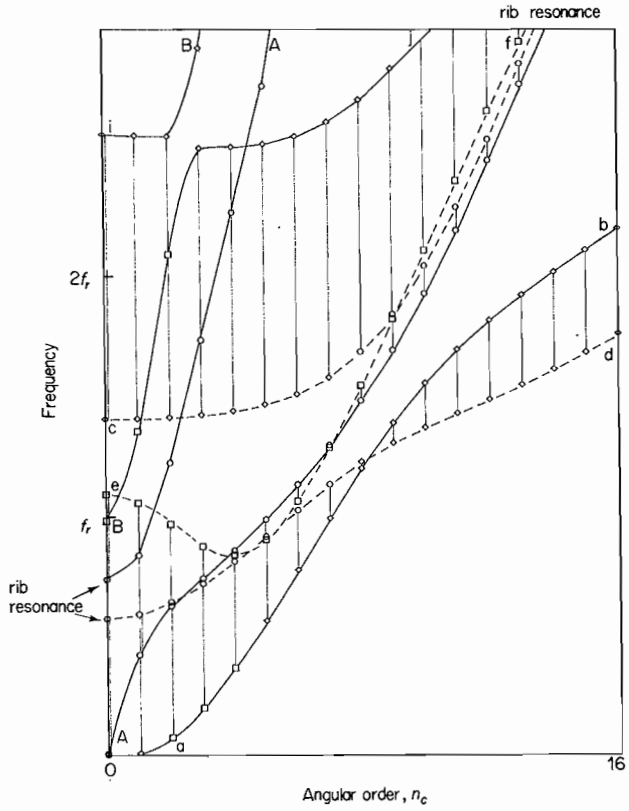

Figure 3. The positions of the pass bands for the ribbed cylinder, for values of n_c from zero to 16. Pass bands are shown as vertical lines. The band edges are joined up by continuous lines, solid for zero Bloch wavenumber and dashed for Nyquist Bloch wavenumber, as an aid to the eye. The narrow band arising from the cantilever rib resonance is indicated. The frequency axis is marked in units of the ring frequency f_r. The cylinder motion associated with these bands and the labelling of their edges is explained in the accompanying paper [5]. The plotting symbols indicate the nature of the motion associated with each point as explained in the text, in the second paragraph of section 5.

is not strong in *any* of our three positions, and the program tends to produce random changes of plotting symbol!

A plot of frequency against n_c for zero and Nyquist axial wavenumber is shown in Figure 3 for the complete theoretical model. In the figure the points have been joined up by continuous lines for zero wavenumber and dashed lines for the Nyquist wavenumber; this is done for the purposes of visual interpretation only. These lines have been given the same labelling as in the accompanying paper, where a qualitative description of the cylinder motion associated with the bands is given. Note that the symbols plotted in the figures are consistent with the modal types indicated in Figure 2 of that paper. The pass bands are indicated by vertical lines joining the points. For this purpose it has been assumed that the band edges occur at zero and Nyquist wavenumbers, which is usually but not always the case, as will be seen shortly. The in-surface branches, where the modal density is low, have been largely ignored. However, the lower edges of the in-surface branches are shown as lines labelled A–A and B–B (the former interacts and mixes with the rib resonance band in the region of $n_c = 1$, where the two lines would otherwise have crossed). The internal structure of the pass bands including that of the in-surface branches may be understood from the more comprehensive plots of frequency against axial wavenumber for individual n_c values to be shown below.

For an interpretation of Figure 3 the reader is referred to section 2 of the accompanying paper in which the qualitative vibration behaviour of a ribbed cylinder is discussed in some detail. Here it is relevant to elaborate on one rather striking feature mentioned

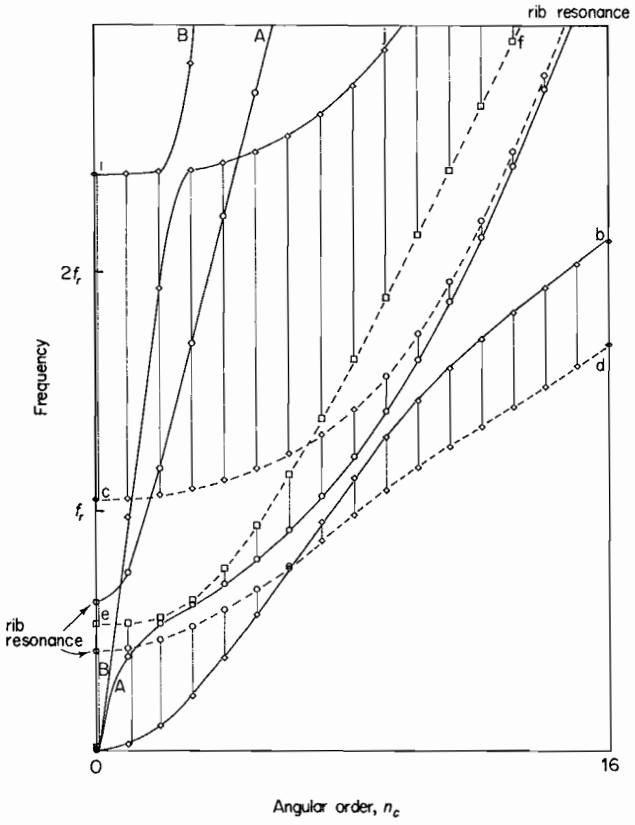

Figure 4. Exactly as Figure 3, with the same rib geometry, but on a flat plate rather than a cylinder.

there. The initial dip in frequency of the line e-f as n_c increases is a result of the asymmetry in rib profile mentioned in section 3.2, and arises in the following way. Line e-f corresponds to a mode at the Nyquist wavenumber for which the rib motion dominates, as can be seen from the square plotting symbol. This motion consists of circumferential bending without axial displacement or twisting, and in principle would include a tangential as well as radial component. However, at this wavenumber the cylindrical shell moves only radially in its lowest mode ($\xi_2 = 0$): any tangential component of the motion would introduce a large shear energy in the shell which can be avoided at the expense of the smaller extensional energy associated with purely radial motion. The constraint $\xi_2 \simeq 0$ defines the neutral axis for bending of the rib where the circumferential extension e_y vanishes: as can be seen from equations (15) and (16) this axis lies a distance a/n_c^2 inside the shell. The bending energy of the rib is a minimum when the neutral axis lies in the flange which, for the dimensions of this particular ribbed cylinder, should happen close to $n_c = 4$. This is where the minimum in line e-f is seen in Figure 3.

It has also been thought worthwhile to show on the same scale the band structure of a ribbed flat plate. This gives an idea of the importance of effects due to cylindricality in the previous results. The plot has been obtained by running the programs for a cylinder of very large radius but with all other dimensions, shell thickness and geometry of rib cross-section, being left the same as for Figure 3. Of course, the modes on a finite cylinder have discrete values of circumferential wavenumber n_c/a, whereas those on a flat plate have a continuous range of corresponding rib trace wavenumbers. In Figure 4 the bands are shown only at discrete trace wavenumbers having the same values as the circumferential wavenumbers in Figure 3. There is general qualitative similarity between Figures 3 and 4, but the frequencies in Figure 3 are systematically higher because the surface of a radially vibrating cylinder has extra stretching energy absent for a flat plate. It is clear that one cannot expect accurate results at these low frequencies from flat-plate modelling of a ribbed cylinder.

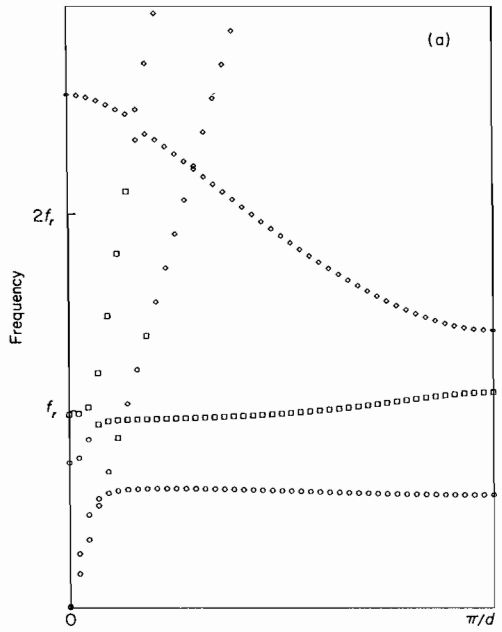

Figure 5. Plots of modal frequency against Bloch wavenumber q along the cylinder axis for the same ribbed cylinder studied in Figure 3, for selected fixed values of n_c: (a) $n_c = 0$; (b) $n_c = 1$; (c) $n_c = 4$; (d) $n_c = 8$; (e) $n_c = 14$. The plotting symbols and marking of the frequency axis are exactly as in Figure 3.

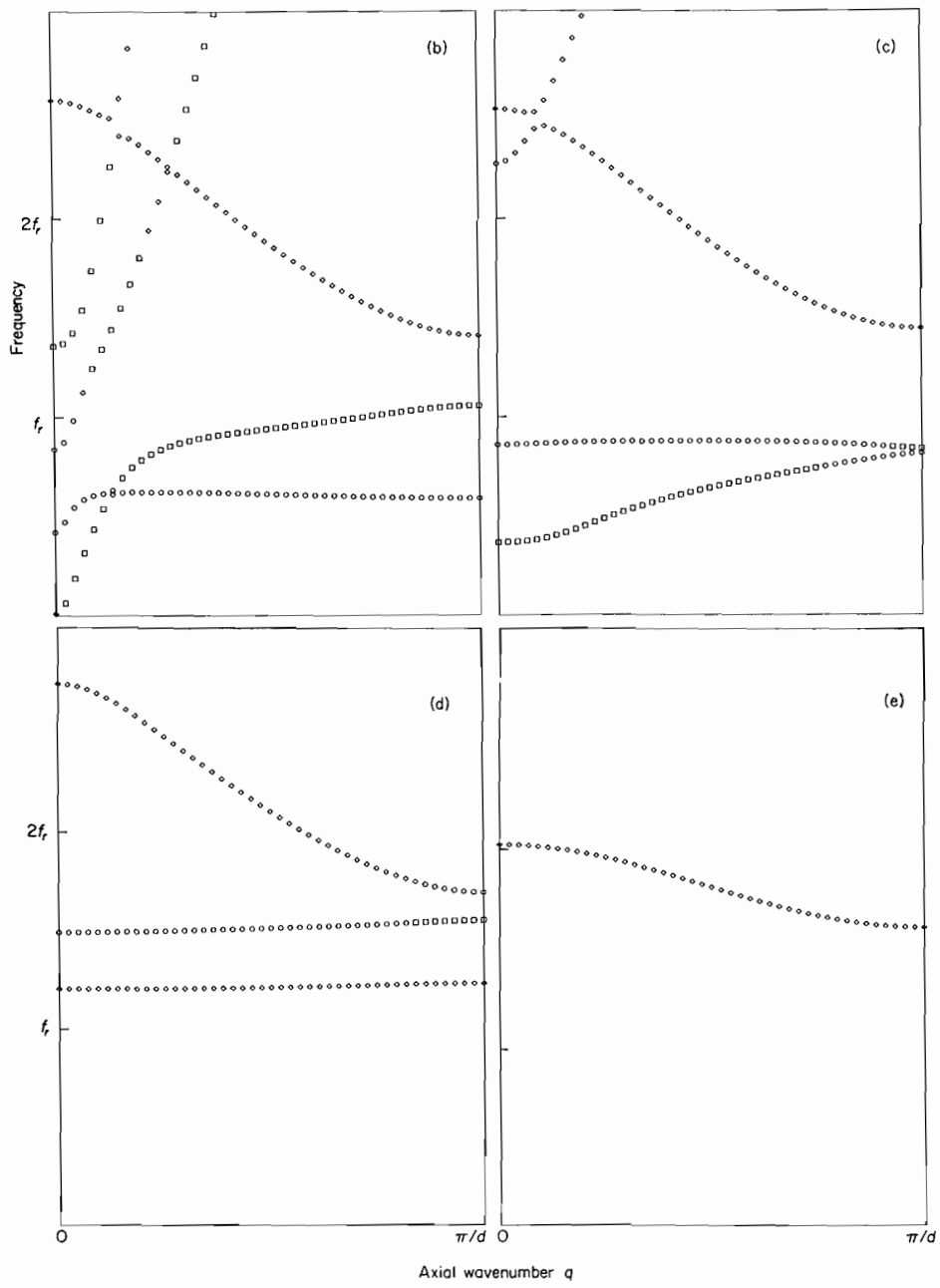

Figure 5 (*cont.*)

The plots of frequency against axial wavenumber q for fixed n_c show the internal structure of the pass bands. Figures 5(a)-(e) show results for selected values of n_c. In these figures one should really be showing continuous dispersion curves since the calculations apply to an infinite cylinder. In fact the results are shown at discrete values $q=(n/44)(\pi/d)$, $n=0$ to 44. These values were chosen to give some idea of the spacing of individual modal frequencies of the experimental ribbed cylinder, which is 44 bays long. The modes for the finite cylinder are of course formed by superposing the forward and backward travelling waves for $+q$ and $-q$ which have the same frequency. The precise modal frequencies of the model will depend on the boundary conditions at the ends of the cylinder, but a proper treatment of that problem lies beyond the scope of

this paper. It is sufficient for present purposes to note that imposing realistic boundary conditions can only shift the individual frequencies of the order of the modal spacing (see for example the discussion of the effect of constraints on mode frequencies given in reference [13], § 92).

The bands in these figures have been plotted with different symbols used to indicate modal character as explained above. Each figure consists in the main of a series of bands of given modal types. Where such bands tend to cross, there is frequently some coupling between the different types of motion which leads to mode mixing and band repulsion. Examples are provided by Figures 5(a) and (b) for $n_c = 0$ and 1, where one sees two bands rising steeply from the origin representing the in-surface compression and shear waves which have high axial velocity. (These are the bands for which the plotting symbols are more confusing than useful, as mentioned above.) These two bands move rapidly out of the top of the figure as n_c increases. The more steeply rising of the two corresponds to axial compression waves, and this couples to the other bands as it passes them through the effect of Poisson's ratio. The less steeply rising branch represents torsional motion, which for $n_c = 0$ does not couple to other branches, although it does couple for $n_c = 1$. Notice that when such coupling and band-repulsion takes place, the extreme frequencies of a given pass band may no longer correspond to zero or Nyquist axial wavenumber, as illustrated for example in Figure 5(a) near the top left corner.

The type of motion in the remaining three bands, two of which have moved out of the top of the figure for $n_c = 14$, is indicated by the square, circle and diamond plotting symbols (see above). As is discussed in the accompanying paper [5], these three remaining bands comprise the rib-resonance band (circles) and the two bands dominated by radial motion of the shell which occur in our frequency range even in the absence of internal rib degrees of freedom (squares and diamonds). Note that in the lowest band radial motion at the ribs is largest at $n_c = 4$ but by $n_c = 8$ radial motion between the ribs has become dominant. This is due to the change of the constraining action of the ribs on the shell from mass-like to spring-like behaviour as n_c increases. For $n_c = 4$ and 8, mode mixing may be seen in the two lowest bands in the vicinity of the Nyquist wavenumber where the plotting symbols change from squares to circles and vice versa. Mode mixing also occurs where the lowest bands try to cross for $n_c = 1$ (Figure 5(b)), but the repulsion effect is small here because the coupling between these bands is weak.

6. CONCLUSIONS

A theory of the vibrations of a ribbed cylinder which is capable of taking into account not only the effects of cylindricality but also internal degrees of freedom (resonances) of the ribs has been presented. The theory predicts the travelling wave solutions on an infinite ribbed cylinder, and gives information about the modal character and distribution of modal frequencies on a long but finite cylinder. The approach taken means that it will be comparatively easy to extend the theory to include effects of fluid loading in future studies.

In this work the cantilever resonance of the rib has been included as an internal degree of freedom. It should be pointed out that for substantially higher frequencies or altered geometries other internal degrees of freedom of rib motion may have to be considered. These could be treated in much the same way as used here for the cantilever resonance.

ACKNOWLEDGMENTS

This work has been carried out with the support of the Procurement Executive, Ministry of Defence. The authors are particularly grateful to Dr I. Roebuck for helpful discussions and much patience during this programme of work. We also thank Professors D. G. Crighton and J. E. Ffowcs Williams for useful comments.

REFERENCES

1. I. D. WILKEN and W. SOEDEL 1976 *Journal of Sound and Vibration* **44**, 563–576. The receptance method applied to ring-stiffened cylinders: analysis of modal characteristics.
2. D. E. BESKOS and J. B. OATES 1981 *Journal of Sound and Vibration* **75**, 1–15. Dynamic analysis of ring-stiffened cylindrical shells.
3. A. A. KOSMODAMINSKII and O. P. TATARINOVA 1981 *Soviet Applied Mechanics* **17**, 456–459. Free vibrations of cylindrical shells reinforced with elastic rings.
4. C. AVALLET and J. PAROT 1982 *Revue du Cethedec* **19**, 159–173. Study of the free wave vibration of ring-stiffened cylindrical shells.
5. C. H. HODGES, J. POWER and J. WOODHOUSE 1985 *Journal of Sound and Vibration* **101**, 237–256. The low frequency vibration of a ribbed cylinder, Part 2: Observations and interpretation.
6. D. J. MEAD and K. K. PUJARA 1971 *Journal of Sound and Vibration* **14**, 525–541. Space harmonic analysis of periodically supported beams: response to convected random loading.
7. R. N. ARNOLD and G. B. WARBURTON 1949 *Proceedings of the Royal Society* **A197**, 238–256. Flexural vibration of the walls of thin cylindrical shells having freely supported ends. (Reprinted in A. KALNINS and C. L. DYM 1976 *Benchmark Papers in Acoustics*, Volume 8, Stroudsberg, Penn: Dowden, Hutchinson and Ross.)
8. L. BRILLOUIN 1946 *Wave Propagation in Periodic Structures.* New York: McGraw Hill. See p. 139 ff.
9. B. R. MACE 1980 *Journal of Sound and Vibration* **73**, 473–486. Periodically stiffened fluid-loaded plates, I: Response to convected harmonic pressure and free wave propagation.
10. B. R. MACE 1980 *Journal of Sound and Vibration* **73**, 487–504. Periodically stiffened fluid-loaded plates, II: Response to line and point forces.
11. D. J. MEAD 1975 *Journal of Sound and Vibration* **40**, 19–39. Wave propagation and natural modes in periodic systems, II: Multi-coupled systems with and without damping.
12. L. CREMER, M. HECKL and E. E. UNGAR 1973 *Structure-Borne Sound.* Berlin: Springer-Verlag.
13. LORD RAYLEIGH 1945 *The Theory of Sound.* New York: Dover.
14. A. E. H. LOVE 1944 *A Treatise on the Mathematical Theory of Elasticity.* New York: Dover. See Chapter XIV.
15. C. H. HODGES, J. POWER and J. WOODHOUSE 1985 *Journal of Sound and Vibration* **101**, 203–218. The use of the sonogram in structural acoustics, and an application to the vibrations of cylindrical shells.

APPENDIX

Here the effect of shear in modifying the modelling of in plane rib bending in section 3.1 is discussed. The effect may be described by a field of shearing displacements $\xi_2^s(x, \theta)$ in the tangential direction which vanish on the middle surface of the shell. These are superposed on the body displacements assumed in shallow rib theory in which there is no shear. In consequence equation (15) for e_y is changed to

$$e_y = \varepsilon_2 - x\kappa_2 + a^{-1}(\partial \xi_2^s / \partial \theta) \tag{A1}$$

while the shear strain is given by

$$e_{xy} = \partial \xi_2^s / \partial x + a^{-1} \xi_2^s. \tag{A2}$$

Now assume a shear displacement profile

$$\xi_2^s = bv(x)\, \mathrm{e}^{\mathrm{i}n_c\theta} \tag{A3}$$

which distributes the shear uniformly through the web but to order t_w/a gives no shear in the flange; i.e.,

$$v(x) = \begin{cases} x & \text{if} \quad x < t_w \\ t_w & \text{if} \quad x > t_w \end{cases}. \tag{A4}$$

With

$$\varepsilon_2 = i\eta\, e^{in_c\theta} \qquad \text{and} \qquad \kappa_2 = i\nu\, e^{in_c\theta} \tag{A5}$$

the potential energy of the rib is

$$S^r_{yx} = \pi Ea \int dx\, l(x)\left\{|\eta - x\nu + bv(x)n_c/a|^2 + \frac{1}{2(1+\sigma)}\, b^*b[v'(x)+v(x)/a]^2\right\}. \tag{A6}$$

This expression may be expanded out in terms of the integrals

$$I_v = \int v(x)l(x)\, dx, \tag{A7}$$

etc. (the same notation as in equation (23) is followed). The terms arising from $|\eta - x\nu|^2$ are those given by equations (24) and (25) in which shear is neglected ($b = 0$). The remaining terms arising from shear are to order t_w/a

$$S^{rs}(\text{shear}) = \pi Ea[(n_c/a)^2 K b^*b + (n_c/a)(\eta I_v - \nu I_{xv})b^* + \text{c.c.}], \tag{A8}$$

$$K = I_{v'}^2 + [a^2/2(1+\sigma)n_c^2]I_{v'^2}. \tag{A9}$$

It is now assumed that b may be determined by static variation: i.e., minimizing equation (A8) without reference to the kinetic energy. This assumption is reasonable since the resonance of the rib web in shear motion has a frequency well above those of interest. The result is

$$b = (\eta I_v - \nu I_{xv})(a/n_c K) \tag{A10}$$

and the total potential energy is then

$$S^{rs} = \eta^*\eta(I_1 - I_v^2/K) - (\eta^*\nu + \nu^*\eta)(I_x - I_{xv}I_v/K) + \nu^*\nu(I_{x^2} - I_{xv}^2/K). \tag{A11}$$

The previous result in which shear is neglected is equivalent to taking these equations in the limit $K \to \infty$ which corresponds to the circumferential wavenumber n/a tending to zero. Clearly shear can be included in equation (25) simply by replacing I_1, I_x, I_{x^2} by the values

$$J_1 = I_1 - I_v^2/K, \qquad J_x = I_x - I_{xv}I_v/K, \qquad J_{x^2} = I_{x^2} - I_{xv}^2/K. \tag{A12}$$

The importance of shear in reducing the bending stiffness of the rib may be estimated by setting $I_v \simeq I_x$, $I_{xv} \simeq I_{x^2}$, $I_{v^2} \simeq I_{x^2}$ since the rib flange is narrow ($t_f \ll t_w$). Thus I_{x^2} which controls the stiffness at large n_c is reduced by a factor

$$J_{x^2}/I_{x^2} = [1 + 2(1+\sigma)n_c^2(t_w/a)^2 R]^{-1}, \tag{A13}$$

where R is approximately the ratio of the cross-sectional area of the rib flange to that of the rib web.